Available online at www.sciencedirect.com
SCIENCE DIRECT®
Comput. Methods Appl. Mech. Engrg. 195 (2006) 1154–1179
Computer methods in applied mechanics and engineering
www.elsevier.com/locate/cma

An entropy-variable-based VMS/GLS method for the simulation of compressible flows on unstructured grids

V. Levasseur [a,*], P. Sagaut [a], F. Chalot [b], A. Davroux [b]

[a] *Laboratoire de Modélisation en Mécanique, Université Pierre et Marie Curie, 4 place Jussieu, Boîte 162, 75252 Paris Cedex 05, France*
[b] *Dassault Aviation—DGT/DTIAE/AERAV, 78 quai Marcel Dassault, 92552 Saint-Cloud Cedex, France*

Received 10 August 2004; accepted 7 April 2005

Abstract

The variational multiscale approach for large-eddy simulation is investigated within a finite element framework. A filtering analog of this method, providing a model, which shares basic structures with hyperviscosity models, is used and evaluated on a freely decaying isotropic turbulence in the limit of infinite Reynolds numbers. The method used is based on a symmetric form of the Navier–Stokes equations stabilized with a Galerkin/least-squares approach. The proposed procedure provides appealing results. It is as satisfactory as the use of Germano and Lilly's dynamic algorithm, without stabilization flaws, and at a lower cost. Comparisons between numerical dissipation and the proper subgrid closure show that the variational multiscale models tend to compute a turbulent viscosity that accounts for the numerical sources of dissipation, which reveals an important feature for an intensive and robust use of VMS-large-eddy simulation.

Keywords: Stabilized finite element methods; Variational multiscale closure; Entropy variables; Large-eddy simulation

1. Introduction

Large-eddy simulation has proven to be a valuable technique for simulating turbulent flows, but most LES research is concentrated on incompressible or subsonic flows computed on structured meshes. First steps on unstructured grids have been made by Jansen [1] while simulating the flow over a NACA 4412

* Corresponding author. Tel.: +33 1 4711 6362; fax: +33 1 4711 4246.
E-mail address: vincent.levasseur@dassault-aviation.fr (V. Levasseur).

0045-7825/$ - see front matter © 2005 Elsevier B.V. All rights reserved.
doi:10.1016/j.cma.2005.04.009

airfoil. Chalot et al. [2] proposed a consistent finite element approach to LES, applied to the decay of isotropic turbulence and a mixing layer. Important development has also been made by Knight et al. [3], whose algorithm has been first tested on decaying isotropic turbulence. Okong'o and Knight [4] and Urbin et al. [5,6] applied it with success to channel flows, boundary layers, and compression corners. Simons and Pletcher [7] compared the results obtained between hexahedral or tetrahedral grids on a decaying isotropic turbulence with different subgrid models, namely MILES, Smagorinsky, and dynamic model.

Besides, to define general methods for closing the LES equations, aiming at a subgrid model able to account for a wide range of subgrid dynamics, multilevel/multiscale approaches have been investigated by many authors. The variational multiscale approach formulated by Hughes et al. [8–11], can be seen as a particular case of two-band decomposition methods. The original key idea is to reconstruct a part of the subgrid modes and to use it as an estimation of the whole subgrid tensor. The subgrid fluctuations being reconstructed on a finer grid than the classical LES grid, there is a priori no restriction on the anisotropy or non-equilibrium of the small scales. Actually, in practice, the same cut-off length is used for the VMS closures as for the classical ones. Thus, the main difference between both modelizations is a change of the dependence of the subgrid dissipation function of the resolved scales on the one hand, and its extent, which is reduced in the case of VMS, on the other hand. This method was shown to yield satisfactory results at low to medium Reynolds numbers in the case of isotropic turbulence and channel flows [10,11]. Holmen et al. [12] reported a high sensitivity of the model with respect to the auxiliary cutoff wavenumber, decreased by the use of a dynamic closure based on Germano and Lilly's procedure. Sagaut and Levasseur observed a spurious pile-up of the resolved kinetic energy when computing isotropic turbulence at high Reynolds numbers in the spectral space [13]. The authors mainly attributed this flaw to the fact that when an orthogonal operator is used to separate large scales from resolved small ones, the distant triadic interactions are neglected. The use of a non-orthogonal filter is advocated to cure this effect by inducing a frequency overlap between the two parts of the resolved flowfield and some direct influence of the closure upon the largest scales. It provides then a model which shares basic features with hyperviscosity models [14].

The present paper aims at investigating this hyperviscosity formulation of the VMS approach in physical space. Koobus and Farhat [15] obtained good results with the original VMS method, with a cell agglomeration technique to separate scales, successfully applied to the flow past a square cylinder on unstructured meshes, showing its viability and possible extension. Another suitable VMS discretization is proposed by Jansen and Tejada-Martinez [16] by the use of a low order hierarchical polynomial expansion basis, and has been applied to decaying isotropic turbulence. A VMS/Galerkin/least-squares method is presented here based on the symmetrized Navier–Stokes equations introduced by Hughes et al. [17], for the simulation of compressible flows on unstructured meshes. The decaying isotropic turbulence in the limit of infinite Reynolds numbers is retained as a test case.

A point of major importance for the development of effective subgrid closures is the coupling between numerical dissipation, especially stabilization techniques in our case, and the subgrid model itself. Two main strategies of modelization can be defined, as presented by Sagaut [18]: the *explicit modeling*, which consists in adding source terms into the equations to account for the subgrid-scales effects, and the *implicit modeling*, which relies on the use of numerical schemes exhibiting errors that play the role of the subgrid model. The variational multiscale approach as proposed by Hughes et al. [9–11] can be seen as a balance between these two strategies, since its original formulation is very close to bubble stabilization, and yet it consists in adding a source term into the evolution equation of the resolved small-scales. It turns out that this method authorizes a computation of the turbulent dissipation, which takes into account numerical dissipation, thanks to the change of dependency of the subgrid tensor upon the largest scales.

The paper is organized as follows: the equations of turbulent compressible flows in entropy variables and the Galerkin/least-squares method are described in Section 2. The different LES closures, with emphasis on the VMS implementation, are detailed in Section 3. The results obtained on a decaying isotropic turbulence test case are presented in Section 4. Finally, conclusions are drawn in Section 5.

2. Governing equations

The case of compressible flows is considered here. For non-hypersonic flows, and considering the local thermodynamic equilibrium hypothesis, the perfect gas relation is supposed to be a proper approximation. The equations are the Navier–Stokes equations for a Newtonian fluid. The filtered equations for large-eddy simulation and the assumptions made are presented in Appendix A.

In this section, we will present the main tenets of the semi-discrete Galerkin/least-squares formulation used for this study. The time integration is carried out using an implicit second order backward difference scheme and second order piecewise linear elements are used for space discretization. The mathematics has been done by Mallet [19] for steady problems and Shakib [20] extended it to the unsteady case. The code used for the study is AETHER, property of Dassault-Aviation (France) and has been mainly developed by Shakib, Johan and Chalot.

2.1. Symmetrized form of the compressible Navier–Stokes equations

The compressible Navier–Stokes equations are symmetrized using the entropy variables introduced by Hughes et al. [17].

In conservation form, the equations can be formally written as

$$\boldsymbol{U}_{,t} + \boldsymbol{F}^{\text{adv}}_{i,i} = \boldsymbol{F}^{\text{diff}}_{i,i}, \tag{1}$$

with

$$\boldsymbol{U} = \rho\begin{Bmatrix} 1 \\ u_1 \\ u_2 \\ u_3 \\ E \end{Bmatrix}; \qquad \boldsymbol{F}^{\text{adv}}_i = \begin{Bmatrix} \rho u_i \\ \rho u_i u_1 + p\delta_{1i} \\ \rho u_i u_2 + p\delta_{2i} \\ \rho u_i u_3 + p\delta_{3i} \\ \rho u_i E + p u_i \end{Bmatrix}; \qquad \boldsymbol{F}^{\text{diff}}_i = \begin{Bmatrix} 0 \\ \sigma_{1i} \\ \sigma_{2i} \\ \sigma_{3i} \\ \sigma_{ij}u_j - q_i \end{Bmatrix}, \tag{2}$$

$\sigma_{ij} = 2\mu S_{ij}(\boldsymbol{u}) = 2\mu\left(\frac{1}{2}(u_{i,j} + u_{j,i}) - \frac{1}{3}u_{k,k}\delta_{ij}\right)$ is the viscous stress, $\mu = \mu(T)$ the molecular viscosity, $q_i = -\kappa T_{,i}$ the heat flux vector, κ and T are respectively the heat conductivity and the temperature, and $E = c_v T + \frac{1}{2}\|\boldsymbol{u}\|^2$ is the specific total energy, with c_v the specific heat at constant volume.

It can be rewritten in a quasi-linear form:

$$\boldsymbol{U}_{,t} + \boldsymbol{A}_i \boldsymbol{U}_{,i} = (\boldsymbol{K}_{ij}\boldsymbol{U}_{,j})_{,i}, \tag{3}$$

where $\boldsymbol{A}_i = \boldsymbol{F}^{\text{adv}}_{i,\boldsymbol{U}}$ is the ith Euler Jacobian matrix, and $\boldsymbol{K} = [\boldsymbol{K}_{ij}]$ is the diffusivity matrix, such that $\boldsymbol{K}_{ij}\boldsymbol{U}_{,j} = \boldsymbol{F}^{\text{diff}}_i$.

We now introduce the generalized entropy function $\mathscr{H}$ defined as

$$\mathscr{H} = \mathscr{H}(\boldsymbol{U}) = -\rho s, \tag{4}$$

with $s = c_v \ln\left(\frac{p}{\rho^\gamma}\right) + s_o$ the entropy per unit mass, and γ the ratio of specific heats.

Then the use of the change of variables $\mathscr{V} : \boldsymbol{U} \mapsto \boldsymbol{V}$ defined by

$$\boldsymbol{V} = \mathscr{V}(\boldsymbol{U}) = \frac{\partial \mathscr{H}^{\mathrm{T}}}{\partial \boldsymbol{U}}, \tag{5}$$

or else, denoting $h = c_p T$ the enthalpy per unit mass, with c_p the specific heat at constant pressure:

$$\boldsymbol{V} = \frac{1}{\rho T}\begin{Bmatrix} -U_5 + \rho c_v T\left(\gamma + 1 - \dfrac{(\gamma-1)s}{r}\right) \\ U_2 \\ U_3 \\ U_4 \\ -U_1 \end{Bmatrix} = \frac{1}{T}\begin{Bmatrix} h - Ts - \dfrac{\|\boldsymbol{u}\|^2}{2} \\ u_1 \\ u_2 \\ u_3 \\ -1 \end{Bmatrix} \tag{6}$$

gives

$$\widetilde{\boldsymbol{A}}_0 \boldsymbol{V}_{,t} + \widetilde{\boldsymbol{A}}_i \boldsymbol{V}_{,i} = (\widetilde{\boldsymbol{K}}_{ij} \boldsymbol{V}_{,j})_{,i}, \tag{7}$$

with

$$\widetilde{\boldsymbol{A}}_0 = \boldsymbol{U}_{,\boldsymbol{V}}, \qquad \widetilde{\boldsymbol{A}}_i = \boldsymbol{A}_i \widetilde{\boldsymbol{A}}_0, \qquad \widetilde{\boldsymbol{K}}_{ij} = \boldsymbol{K}_{ij} \widetilde{\boldsymbol{A}}_0. \tag{8}$$

All matrices $\widetilde{\boldsymbol{A}}_0$, $\widetilde{\boldsymbol{A}}_i$, $\widetilde{\boldsymbol{K}} = [\widetilde{\boldsymbol{K}}_{ij}]$ are symmetric, $\widetilde{\boldsymbol{A}}_0$ is positive-definite, and $\widetilde{\boldsymbol{K}}$ is positive-semidefinite. Thus, this formulation, Eq. (7), possesses advantageous mathematical properties, used in the numerical solution of the equations; it also makes physical sense in that the Clausius–Duhem inequality is automatically satisfied (see [17] or [19] for details). $\widetilde{\boldsymbol{K}}_{ij}$ and $\boldsymbol{K}_{ij}$ are both functions of μ, κ, and $\boldsymbol{U}$ (or $\boldsymbol{V}$). The expressions of $\widetilde{\boldsymbol{A}}_0$, $\widetilde{\boldsymbol{A}}_i$ and $\widetilde{\boldsymbol{K}}_{ij}$ are given in Appendix B.

2.2. LES equations in entropy variables

The large-eddy simulation consists in projecting the DNS solution onto a basis with fewer degrees of freedom, resulting in a filtering of the small scales. When resolving in entropy variables, two different approaches are possible: whether filter the conservation equations, and then apply the change of variables $\mathscr{V}$, or directly solve the problem for the filtered entropy variables. Since $\mathscr{V}$ is non-linear these approaches will not lead to the same systems of equations, although they should be equivalent. The first approach is preferred because it preserves the same structure of the LES equations in entropy variables as in conservative variables. In particular, the subgrid terms will be exactly the same.

Using the usual mass-weighted change of variables to filter the conservative variables, let us now define:

$$\widehat{\boldsymbol{V}}^{\mathrm{T}} = \frac{\partial \mathscr{H}(\overline{\boldsymbol{U}})}{\partial \overline{\boldsymbol{U}}}, \tag{9}$$

$$\widehat{\boldsymbol{A}}_0 = \overline{\boldsymbol{U}}_{,\widehat{\boldsymbol{V}}}, \tag{10}$$

$$\widehat{\boldsymbol{A}}_i = \overline{\boldsymbol{A}}_i \widehat{\boldsymbol{A}}_0, \tag{11}$$

$$\widehat{\boldsymbol{K}}_{ij} = \overline{\boldsymbol{K}}_{ij} \widehat{\boldsymbol{A}}_0, \tag{12}$$

where

$$\overline{\boldsymbol{U}} = \begin{Bmatrix} \bar{\rho} \\ \overline{\rho u_1} \\ \overline{\rho u_2} \\ \overline{\rho u_3} \\ \overline{\rho E} \end{Bmatrix} = \bar{\rho}\begin{Bmatrix} 1 \\ \tilde{u}_1 \\ \tilde{u}_2 \\ \tilde{u}_3 \\ \widetilde{E} \end{Bmatrix} \quad \text{is the filtered counterpart of } \boldsymbol{U}. \tag{13}$$

Note that here, $\widehat{\boldsymbol{V}}$ is not the low frequency part of $\boldsymbol{V}$: $\widehat{\boldsymbol{V}} = \frac{\partial \mathscr{H}(\overline{\boldsymbol{U}})}{\partial \overline{\boldsymbol{U}}} \neq \overline{\boldsymbol{V}} = \overline{\frac{\partial \mathscr{H}(\boldsymbol{U})}{\partial \boldsymbol{U}}}$.

The following relationships are then satisfied:

$$\tilde{u}_i = \overline{\rho u_i}/\overline{\rho} = -\frac{\widehat{\boldsymbol{V}}_{i+1}}{\widehat{\boldsymbol{V}}_5}, \tag{14}$$

$$\widetilde{T} = \overline{\rho T}/\overline{\rho} = -\frac{1}{\widehat{\boldsymbol{V}}_5}, \tag{15}$$

and

$$\widehat{\boldsymbol{V}} = \frac{1}{\bar{\rho}\widetilde{T}}\begin{Bmatrix} -\overline{U}_5 + \bar{\rho}c_v\widetilde{T}\left(\gamma + 1 - \dfrac{(\gamma-1)\tilde{s}}{r}\right) \\ \overline{U}_2 \\ \overline{U}_3 \\ \overline{U}_4 \\ -\overline{U}_1 \end{Bmatrix} = \frac{1}{\widetilde{T}}\begin{Bmatrix} \tilde{h} - \widetilde{T}\tilde{s} - \dfrac{\|\tilde{\boldsymbol{u}}\|^2}{2} \\ \tilde{u}_1 \\ \tilde{u}_2 \\ \tilde{u}_3 \\ -1 \end{Bmatrix}, \tag{16}$$

where $\tilde{u}_i$ and $\widetilde{T}$ are respectively the filtered velocity and the filtered temperature fields.

Then filtering Eq. (3) gives

$$\overline{\boldsymbol{U}}_{,t} + \overline{\boldsymbol{A}_i\boldsymbol{U}_{,i}} = \overline{\left(\boldsymbol{K}_{ij}\boldsymbol{U}_{,j}\right)_{,i}}. \tag{17}$$

Assuming that the filtering operation commutes with time and space derivatives, one can write

$$\overline{\boldsymbol{U}}_{,t} + \overline{\boldsymbol{A}}_i\overline{\boldsymbol{U}}_{,i} = \left(\overline{\boldsymbol{K}}_{ij}\overline{\boldsymbol{U}}_{,j}\right)_{,i} \underbrace{-\left(\overline{\boldsymbol{A}_i\boldsymbol{U}_{,i}} - \overline{\boldsymbol{A}}_i\overline{\boldsymbol{U}}_{,i}\right) + \left(\overline{\boldsymbol{K}_{ij}\boldsymbol{U}_{,j}} - \overline{\boldsymbol{K}}_{ij}\overline{\boldsymbol{U}}_{,j}\right)_{,i}}_{\text{subgrid terms}}. \tag{18}$$

Henceforth, introducing the entropy variables $\widehat{\boldsymbol{V}}$:

$$\widehat{\boldsymbol{A}}_0\widehat{\boldsymbol{V}}_{,t} + \widehat{\boldsymbol{A}}_i\widehat{\boldsymbol{V}}_{,i} = \left(\widehat{\boldsymbol{K}}_{ij}\widehat{\boldsymbol{V}}_{,j}\right)_{,i} - \left(\overline{\boldsymbol{A}_i\boldsymbol{U}_{,i}} - \overline{\boldsymbol{A}}_i\overline{\boldsymbol{U}}_{,i}\right) + \left(\overline{\boldsymbol{K}_{ij}\boldsymbol{U}_{,j}} - \overline{\boldsymbol{K}}_{ij}\overline{\boldsymbol{U}}_{,j}\right)_{,i} \tag{19}$$

$$= \left(\widehat{\boldsymbol{K}}_{ij}\widehat{\boldsymbol{V}}_{,j}\right)_{,i} \underbrace{-\left(\widetilde{\boldsymbol{A}_i\boldsymbol{V}}_{,i} - \widehat{\boldsymbol{A}}_i\widehat{\boldsymbol{V}}_{,i}\right) + \left(\widetilde{\boldsymbol{K}_{ij}\boldsymbol{V}}_{,j} - \widehat{\boldsymbol{K}}_{ij}\widehat{\boldsymbol{V}}_{,j}\right)_{,i}}_{\text{subgrid terms}}. \tag{20}$$

The subgrid terms represent the effect of the unresolved scales on the filtered flowfield, and are not directly computable. Following the results of Vreman et al. [21] within the context of a priori tests on DNS of a temporal mixing layer, the non-linearity associated with viscous stress and heat flux, namely the diffusive fluxes $\left(\overline{\boldsymbol{K}_{ij}\boldsymbol{U}_{,j}}\right)_{,i} - \left(\overline{\boldsymbol{K}}_{ij}\overline{\boldsymbol{U}}_{,j}\right)_{,i}$ in Eq. (19), are assumed negligible. Eventually, within the assumptions detailed in Appendix A, the remaining subgrid terms are modeled as a diffusive term and the LES equation system written in entropy variables becomes,

$$\widehat{\boldsymbol{A}}_0\widehat{\boldsymbol{V}}_{,t} + \widehat{\boldsymbol{A}}_i\widehat{\boldsymbol{V}}_{,i} = \left(\left(\widehat{\boldsymbol{K}}_{ij} + \widehat{\boldsymbol{K}}_{ij}^{\mathrm{SGS}}\right)\widehat{\boldsymbol{V}}_{,j}\right)_{,i}, \tag{21}$$

where

$$\widehat{\boldsymbol{K}}_{ij}^{\mathrm{SGS}} = \widehat{\boldsymbol{K}}_{ij}(\mu_t, \kappa_t, \widehat{\boldsymbol{U}}), \tag{22}$$

so that the large-eddy simulation consists in adding a source term that is the exact diffusive contribution, except that μ and κ are substituted with their turbulent analog μ_t and κ_t.

2.3. The Galerkin/least-squares formulation

Considering a domain Ω, and its boundary Γ, discretized with n_{el} elements Ω_e, the semi-discrete Galerkin/least-squares formulation of Eq. (21) reads,

$$\begin{aligned}
&\int_\Omega \left(\boldsymbol{W}^h \cdot \widehat{\boldsymbol{A}}_0 \widehat{\boldsymbol{V}}^h_{,t} - \boldsymbol{W}^h_{,i} \cdot \widehat{\boldsymbol{F}}^{\mathrm{adv}}_i(\widehat{\boldsymbol{V}}^h) + \boldsymbol{W}^h_{,i} \cdot (\widehat{\boldsymbol{K}}_{ij} + \widehat{\boldsymbol{K}}^{\mathrm{SGS}}_{ij}) \cdot \widehat{\boldsymbol{V}}^h_{,j} \right) \mathrm{d}\Omega \\
&\quad + \int_\Gamma \left(\boldsymbol{W}^h \cdot \left(\widehat{\boldsymbol{F}}_i(\widehat{V}^h) - (\widehat{\boldsymbol{K}}_{ij} + \widehat{\boldsymbol{K}}^{\mathrm{T}}_{ij}) \boldsymbol{V}^h_{,j} \right) \right) n_i \, \mathrm{d}\Gamma \\
&\quad + \sum_{e=1}^{n_{el}} \int_{\Omega_e} \mathscr{L}(\mathbf{W}^h) \boldsymbol{\tau} \left(\widehat{\boldsymbol{A}}_0 \widehat{\boldsymbol{V}}^h_{,t} + \mathscr{L}(\widehat{\boldsymbol{V}}^h) \right) \mathrm{d}\Omega_e = 0,
\end{aligned} \tag{23}$$

with $\mathscr{L}(\widehat{\boldsymbol{V}}) = \widehat{\boldsymbol{A}}_i \frac{\partial \widehat{\boldsymbol{V}}}{\partial x_i} - \frac{\partial}{\partial x_i} \left((\widehat{\boldsymbol{K}}_{ij} + \widehat{\boldsymbol{K}}^{\mathrm{SGS}}_{ij}) \frac{\partial \widehat{\boldsymbol{V}}}{\partial x_j} \right)$ the steady compressible Navier–Stokes operator, $\boldsymbol{W}$ a test function, and $\boldsymbol{\tau}$ a characteristic time-scale matrix.

It is well known that the least-squares stabilization, when applied to a steady scalar advection–diffusion equation, is equivalent to the adjunction of an artificial viscosity, $\kappa_{\mathrm{num}} = \tau |u|^2 = f(Pe)|u|h/2$, where $f(Pe)$ is a function of the Peclet number $|u|h/2\kappa$ which controls the stability of advection-dominated zones of the flow. This has been generalized for the Navier–Stokes equations so that the added numerical viscosity vanishes when the Peclet number is low. A similar mechanism is incorporated in the definition of the $\boldsymbol{\tau}$ matrix. For unsteady cases, the term $\widehat{\boldsymbol{A}}_0 \widehat{\boldsymbol{V}}^h_{,t}$ has been added to the residual to be consistent and to enable the residual to vanish to 0, as the solution converges, but the chosen test function remains $\mathscr{L}(\boldsymbol{W}^h)$ as in steady case. The formulation turns out to be much more dissipative otherwise.

Note that when using piecewise linear elements, the second-order derivative terms appearing in the definition of the least-squares stabilization have zero value. However, it is possible to easily reconstruct them in order to improve the consistency of the formulation (see [22] for details). Such a reconstruction algorithm has been implemented in the code but it does not bring any improvement in the case of a freely evolving isotropic turbulence at high Reynolds number.

2.3.1. Definition of the characteristic time-scale matrix $\boldsymbol{\tau}$

The structure of the $\boldsymbol{\tau}$ matrix is a major point of this Galerkin/least-squares formulation. Studies of simple one-dimensional problems, linear error estimates, dimensional analysis and convergence proofs provide a few conditions to satisfy for the design of $\boldsymbol{\tau}$, but are not sufficient to define a unique characteristic time-scale matrix. Mallet et al. [23,19] give a general structure of $\boldsymbol{\tau}$ for the steady Navier–Stokes equations, and Shakib [20] extended it to the unsteady case.

The $\boldsymbol{\tau}$ matrix is decomposed into an advective part and a diffusive correction. Shakib proposed the following definition for the advective part:

$$\boldsymbol{\tau}^{\mathrm{adv}} = \widetilde{\boldsymbol{A}}_0^{-1} \left[\left(\frac{\partial \xi_0}{\partial x_0} \right)^2 \mathbf{1}_{n_{\mathrm{dof}}} + \left(\frac{\partial \xi_i}{\partial x_j} \frac{\partial \xi_i}{\partial x_k} \right) \boldsymbol{A}_j \boldsymbol{A}_k \right]^{-1/2}, \tag{24}$$

where n_{dof} is the number of degrees of freedom, and ξ_0 and ξ_i denote the local space-time coordinates, the index 0 being related to time "direction".

We will refer to the above references for further details about the definition and properties of the characteristic time scale matrix $\boldsymbol{\tau}$.

3. Subgrid closures

3.1. Smagorinsky model

Following Kolmogorov's dimensional analysis (1941) a characteristic time for turbulence can be written as $T = (\Delta^2/\varepsilon)^{1/3}$, where ε is the energy transfer rate within the inertial range, and Δ is the size of the smallest resolved scale. Thus, the turbulent viscosity is expressed as

$$\nu_t \propto \varepsilon^{1/3}\Delta^{4/3}. \tag{25}$$

The reader is referred to Pope [24], for instance, for further details on Kolmogorov's work.

Smagorinsky [25] proposed then a local equilibrium hypothesis, which implies that the energy transfer rate is equal to the subgrid dissipation. The eddy viscosity appears thus as a function of the resolved velocity field:

$$\nu_t = (C_S\Delta)^2|S(\tilde{\boldsymbol{u}})| = (C_S\Delta)^2\sqrt{2S_{ij}(\tilde{\boldsymbol{u}})S_{ij}(\tilde{\boldsymbol{u}})}. \tag{26}$$

A way to alleviate the classic shortcomings of the Smagorinsky model, mainly an overdissipative behavior, is the use of the Germano procedure which enables the adaptation of the turbulent viscosity to the local property of the flow by computing a time- and space-dependent Smagorinsky constant [26]. This procedure can be applied to any subgrid model that relies on the use of a constant. When applied to the Smagorinsky closure, the resulting model is historically referred to as the dynamic model.

3.2. The variational multiscale approach

The Smagorinsky model is known to yield good results in isotropic turbulence. However, it turns out to be inadequate to non-homogeneous flows because it assumes that ensuring the correct balance of resolved kinetic energy is enough to account for the effect of unresolved scales on the large structures. The Germano and Lilly's dynamic procedure alleviates this difficulty but introduces instabilities only resolved by averaging in homogeneous directions. This is the major drawback of this technique, which renders its use really problematic on unstructured meshes.

Instead of adapting the constant of the Smagorinsky model, an alternative could be to change the dependence of the model upon the resolved scales. Thus, to define a more general model, Hughes et al. [9–11] proposed to rebuild a part of the subgrid modes and to use these reconstructed modes as an estimation for the whole subgrid motion. The original formulation relies on two key hypotheses:

- An a priori variational projection is used to differentiate the resolved scales;
- The resolved large scales and the subgrid scales are supposed distant enough so that they do not directly interact.

A schematic view of the scale separation is presented on Fig. 1 by the way of a spectral cut-off. The wavenumber k_c' is associated with the mesh size Δ, and k_c corresponds to Δ'' which is a characteristic length of the resolved scales separation. The choice of a correct Δ'' is further discussed at the end of the section. $\boldsymbol{u}^{\mathrm{R}}$ represents the total resolved velocity field, decomposed into $\widetilde{\boldsymbol{u}}$ and $\boldsymbol{u}''$ respectively the low- and high-frequency parts. $\boldsymbol{u}' = \boldsymbol{u} - \widetilde{\boldsymbol{u}}$ corresponds to the fluctuation part associated with the primary LES cut-off k_c. Remember that the filtered velocity field $\widetilde{\boldsymbol{u}}$ is associated with the filtered conservative-variable vector $\overline{\boldsymbol{U}}$ via Favre averaging, Eq. (13).

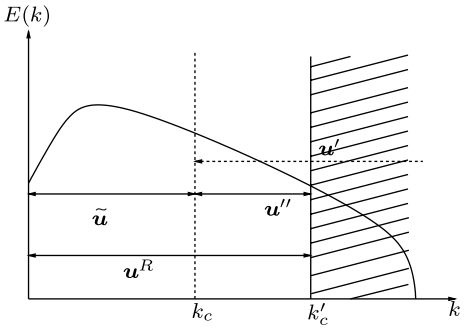

Fig. 1. Schematic view of the variational multiscale approach on a kinetic energy spectrum.

For compressible flows, the vectors associated with the conservative variables verify the relations: $\boldsymbol{U} = \overline{\boldsymbol{U}} + \boldsymbol{U}'$, $\boldsymbol{U}^{\mathrm{R}} = \overline{\boldsymbol{U}} + \boldsymbol{U}''$, and $\boldsymbol{U}'' = (\boldsymbol{U}^{\mathrm{R}})'$. A precise definition of how to differentiate the total resolved scales from $\boldsymbol{U}^{\mathrm{R}}$ into $\overline{\boldsymbol{U}}$ and $\boldsymbol{U}''$ is proposed in the following (see Eq. (43)). Let us introduce now the entropy variables counterparts: $\widehat{\boldsymbol{V}} = \mathscr{V}(\overline{\boldsymbol{U}})$, $\boldsymbol{V}' = \mathscr{V}(\boldsymbol{U}')$, $\boldsymbol{V}'' = \mathscr{V}(\boldsymbol{U}'')$, $\boldsymbol{V}^{\mathrm{R}} = \mathscr{V}(\boldsymbol{U}^{\mathrm{R}})$.

To ease the notations, similar exponents (prime, double prime and R) are used for conservative or entropy variables, though they do not have the same meaning, as it was underlined above.

We describe below the original formulation of the VMS/LES within a filtering framework. By these means, the problem can be handled by the solution of a unique equation for $\boldsymbol{V}^{\mathrm{R}}$ instead of two different equations in the original VMS, respectively for large- and small-scale motions $\widehat{\boldsymbol{V}}$ and $\boldsymbol{V}''$. Moreover, it enables not to increase the number of degrees of freedom of the problem. Vreman [27] detailed it in the case of incompressible fluids, and it is generalized here for compressible flows in entropy variables.

First of all, the total resolved field $\boldsymbol{V}^{\mathrm{R}}$ satisfies the following equation:

$$\boldsymbol{A}_0^{\mathrm{R}} \boldsymbol{V}^{\mathrm{R}}_{,t} + \boldsymbol{A}_i^{\mathrm{R}} \boldsymbol{V}^{\mathrm{R}}_{,i} = \left(\boldsymbol{K}_{ij}^{\mathrm{R}} \boldsymbol{V}^{\mathrm{R}}_{,j}\right)_{,i} - \left((\widetilde{\boldsymbol{A}}_i \boldsymbol{V}_{,i})^{\mathrm{R}} - \boldsymbol{A}_i^{\mathrm{R}} \boldsymbol{V}^{\mathrm{R}}_{,i}\right) + \left((\widetilde{\boldsymbol{K}}_{ij} \boldsymbol{V}_{,j})^{\mathrm{R}} - \boldsymbol{K}_{ij}^{\mathrm{R}} \boldsymbol{V}^{\mathrm{R}}_{,j}\right). \tag{27}$$

We will note $\boldsymbol{\tau}_s = \left((\widetilde{\boldsymbol{A}}_i \boldsymbol{V}_{,i})^{\mathrm{R}} - \boldsymbol{A}_i^{\mathrm{R}} \boldsymbol{V}^{\mathrm{R}}_{,i}\right) - \left((\widetilde{\boldsymbol{K}}_{ij} \boldsymbol{V}_{,j})^{\mathrm{R}} - \boldsymbol{K}_{ij}^{\mathrm{R}} \boldsymbol{V}^{\mathrm{R}}_{,j}\right)$ the subgrid term corresponding to this finest level of filtering.

The equation for the largest scales of motion is

$$\widehat{\boldsymbol{A}}_0 \widehat{\boldsymbol{V}}_{,t} + \widehat{\boldsymbol{A}}_i \widehat{\boldsymbol{V}}_{,i} = (\widehat{\boldsymbol{K}}_{ij} \widehat{\boldsymbol{V}}_{,j})_{,i} - (\overline{\widetilde{\boldsymbol{A}}_i \boldsymbol{V}_{,i}} - \widehat{\boldsymbol{A}}_i \widehat{\boldsymbol{V}}_{,i}) + (\overline{\widetilde{\boldsymbol{K}}_{ij} \boldsymbol{V}_{,j}} - \widehat{\boldsymbol{K}}_{ij} \widehat{\boldsymbol{V}}_{,j})_{,i}. \tag{28}$$

The subgrid terms in Eq. (28), noted $\boldsymbol{T}_s$, can be divided into two parts:

$$\boldsymbol{T}_s = (\overline{\widetilde{\boldsymbol{A}}_i \boldsymbol{V}_{,i}} - \widehat{\boldsymbol{A}}_i \widehat{\boldsymbol{V}}_{,i}) - (\overline{\widetilde{\boldsymbol{K}}_{ij} \boldsymbol{V}_{,j}} - \widehat{\boldsymbol{K}}_{ij} \widehat{\boldsymbol{V}}_{,j})_{,i} = \widehat{\mathscr{B}}_1(\widehat{\boldsymbol{V}}, \boldsymbol{V}^{\mathrm{R}}) + \widehat{\mathscr{B}}_2(\boldsymbol{V}, \boldsymbol{V}^{\mathrm{R}}), \tag{29}$$

where

$$\widehat{\mathscr{B}}_1(\widehat{\boldsymbol{V}}, \boldsymbol{V}^{\mathrm{R}}) = (\overline{\boldsymbol{A}_i^{\mathrm{R}} \boldsymbol{V}^{\mathrm{R}}_{,i}} - \widehat{\boldsymbol{A}}_i \widehat{\boldsymbol{V}}_{,i}) - (\overline{\boldsymbol{K}_{ij}^{\mathrm{R}} \boldsymbol{V}^{\mathrm{R}}_{,j}} - \widehat{\boldsymbol{K}}_{ij} \widehat{\boldsymbol{V}}_{,j})_{,i}, \tag{30}$$

$$\widehat{\mathscr{B}}_2(\boldsymbol{V}, \boldsymbol{V}^{\mathrm{R}}) = (\overline{\widetilde{\boldsymbol{A}}_i \boldsymbol{V}_{,i}} - \overline{\boldsymbol{A}_i^{\mathrm{R}} \boldsymbol{V}^{\mathrm{R}}_{,i}}) - (\overline{\widetilde{\boldsymbol{K}}_{ij} \boldsymbol{V}_{,j}} - \overline{\boldsymbol{K}_{ij}^{\mathrm{R}} \boldsymbol{V}^{\mathrm{R}}_{,j}})_{,i} = \widehat{\boldsymbol{\tau}}_s. \tag{31}$$

$\widehat{\mathscr{B}}_1$ and $\widehat{\mathscr{B}}_2$ represent the effects on the large-scale motion respectively of the resolved small scales (modes $k \in [k_c, k'_c]$ on Fig. 1) and the subgrid scales (modes $k \geqslant k'_c$).

In the same way, the equation for the resolved small scales writes:

$$\boldsymbol{A}_0'' \boldsymbol{V}''_{,t} + \boldsymbol{A}_i'' \boldsymbol{V}''_{,i} = (\boldsymbol{K}_{ij}'' \boldsymbol{V}''_{,j})_{,i} - \mathscr{B}_1''(\boldsymbol{V}'', \boldsymbol{V}^{\mathrm{R}}) - \mathscr{B}_2''(\boldsymbol{V}, \boldsymbol{V}^{\mathrm{R}}), \tag{32}$$

where

$$\mathscr{B}_1''(\boldsymbol{V}'', \boldsymbol{V}^{\mathrm{R}}) = \left((\boldsymbol{A}_i^{\mathrm{R}} \boldsymbol{V}_{,i}^{\mathrm{R}})' - \boldsymbol{A}_i'' \boldsymbol{V}_{,i}''\right) - \left((\boldsymbol{K}_{ij}^{\mathrm{R}} \boldsymbol{V}_{,j}^{\mathrm{R}})' - \boldsymbol{K}_{ij}'' \boldsymbol{V}_{,j}''\right)_{,i}, \tag{33}$$

$$\mathscr{B}_2''(\boldsymbol{V}, \boldsymbol{V}^{\mathrm{R}}) = \left((\widetilde{\boldsymbol{A}}_i \boldsymbol{V}_{,i})'' - (\boldsymbol{A}_i^{\mathrm{R}} \boldsymbol{V}_{,i}^{\mathrm{R}})'\right) - \left((\widetilde{\boldsymbol{K}}_{ij} \boldsymbol{V}_{,j})'' - (\boldsymbol{K}_{ij}^{\mathrm{R}} \boldsymbol{V}_{,j}^{\mathrm{R}})'\right)_{,i} = \boldsymbol{\tau}_s''. \tag{34}$$

$\mathscr{B}_1''$ and $\mathscr{B}_2''$ represent the interactions of the resolved small scales respectively with the smallest frequencies and the subgrid modes.

The key idea for the VMS modelization is to neglect the distant kinetic energy transfers involving the large scales and the subgrid scales, namely to neglect $\widehat{\mathscr{B}}_2 = \widehat{\boldsymbol{\tau}}_s$. Therefore, when summing Eqs. (28) and (32), we find the evolution equation of the total resolved field in entropy variables:

$$\boldsymbol{A}_0^{\mathrm{R}} \boldsymbol{V}_{,t}^{\mathrm{R}} + \boldsymbol{A}_i^{\mathrm{R}} \boldsymbol{V}_{,i}^{\mathrm{R}} = (\boldsymbol{K}_{ij}^{\mathrm{R}} \boldsymbol{V}_{,j}^{\mathrm{R}})_{,i} - \mathscr{B}_2''(\boldsymbol{V}, \boldsymbol{V}^{\mathrm{R}}). \tag{35}$$

$\mathscr{B}_2''$ remains unresolved, and needs therefore to be modeled. In conservative variables, the effect of the subgrid scales on the resolved small scales is accounted for in the momentum equations by analogy with the usual turbulent viscosity hypothesis:

$$\tau_{s_{ij}}'' - \tfrac{1}{3}\tau_{s_{kk}}'' \delta_{ij} = -2\mu_t S_{ij}(\boldsymbol{u}''), \tag{36}$$

where $\tau_{s_{ij,j}}'' = \mathscr{B}_2''\rfloor_{i+1}$ (e.g., the $(i+1)$th component of $\mathscr{B}_2''$) for $i = 1,3$ are the subgrid terms in the momentum equations and the two eddy-viscosities studied in the paper are Smagorinsky-like models:

$$\nu_t = (C_1 \Delta)^2 |S(\boldsymbol{u}'')| \tag{37}$$

and

$$\nu_t = (C_2 \Delta)^2 |S(\widetilde{\boldsymbol{u}})|, \tag{38}$$

where $\Delta \sim \pi/k_c'$ is the mesh size.

The two models defined by Eqs. (37) and (38) are referred to as the Small–Small and the Large–Small model. Note that the eddy-viscosity $\nu_t = (C\Delta)^2 |S(\boldsymbol{u}^{\mathrm{R}})|$ has also been tested but the results obtained with this closure are not presented here. It turns out to be a little too dissipative and it should probably incorporate a dynamic algorithm such as Holmen et al. do [12].

The same modelization as the classical LES is kept for the turbulent heat flux by introducing a turbulent heat conductivity such that: $\kappa_t = \gamma c_v \mu_t / Pr_t$, with Pr_t is the turbulent Prandtl number set equal to 0.9.

As a result, the equation of the filtering multiscale LES in entropy variables writes:

$$\boldsymbol{A}_0^{\mathrm{R}} \boldsymbol{V}_{,t}^{\mathrm{R}} + \boldsymbol{A}_i^{\mathrm{R}} \boldsymbol{V}_i^{\mathrm{R}} = \left(\boldsymbol{K}_{ij}^{\mathrm{R}} \boldsymbol{V}_{,j}^{\mathrm{R}}\right)_{,i} + (\boldsymbol{K}_{ij}^{\mathrm{VMS}} \boldsymbol{V}_{,j}^{\mathrm{VMS}})_{,i}, \tag{39}$$

where $\boldsymbol{K}_{ij}^{\mathrm{VMS}} = \boldsymbol{K}_{ij}(\mu_t, \kappa_t, \boldsymbol{u}'', T^{\mathrm{R}})$, and

$$\boldsymbol{V}^{\mathrm{VMS}} = \frac{1}{T^{\mathrm{R}}} \begin{Bmatrix} T^{\mathrm{R}} V_1^{\mathrm{R}} \\ \tilde{u}_1'' \\ \tilde{u}_2'' \\ \tilde{u}_3'' \\ -1 \end{Bmatrix}. \tag{40}$$

Sagaut and Levasseur [13] reported a spurious kinetic-energy pile-up in the case of incompressible freely evolving isotropic turbulence in the limit of an infinite Reynolds number. The use of a non-orthogonal operator was proved to cure this problem by making all the scales sensitive to the subgrid closure. Using a second-order Taylor expansion for the Gaussian filter, the reconstructed modes of the velocity field can be

written as: $\boldsymbol{u}'' = -\frac{\Delta''}{24}\nabla^2\boldsymbol{u}^{\mathrm{R}}$, with $\Delta'' \sim \pi/k_c$ a characteristic length of the resolved scales separation. The choice of Δ'' will be further discussed in the following. The variational multiscale modelization for the subgrid stress thus becomes:

$$\boldsymbol{\tau} = -2\mu_t S(\boldsymbol{u}'') = -2\bar{\rho}C_1\Delta^2|S(\boldsymbol{u}'')|S(\boldsymbol{u}'') = -2\bar{\rho}C_1'\Delta^6|S(\nabla^2\boldsymbol{u}^{\mathrm{R}})|S(\nabla^2\boldsymbol{u}^{\mathrm{R}}) \quad \text{Small–Small}, \tag{41}$$

$$\boldsymbol{\tau} = -2\mu_t S(\boldsymbol{u}'') = -2\bar{\rho}C_2\Delta^2|S(\widetilde{\boldsymbol{u}})|S(\boldsymbol{u}'') = -2\bar{\rho}C_2'\Delta^4|S(\widetilde{\boldsymbol{u}})|S(\nabla^2\boldsymbol{u}^{\mathrm{R}}) \quad \text{Large–Small}. \tag{42}$$

Practically, the small scales velocity field $\boldsymbol{u}''$ is computed thanks to an integration by part similar to that of the viscous terms. Thus, one can obtain

$$\boldsymbol{u}''_A = \frac{\Delta''^2}{24}M^{AA^{-1}}\sum_B\left(\int_\Omega N_{A,i}N_{B,i}\,\mathrm{d}\Omega - \int_\Gamma N_A N_{B,i}n_i\,\mathrm{d}\Gamma\right)\boldsymbol{u}^{\mathrm{R}}_B, \tag{43}$$

where M^{AA} is the special lumped mass matrix advocated by Hughes [28], and defined for its elementary part as

$$M_e^{AB^L} = \begin{cases} \dfrac{\displaystyle\int_{\Omega_e} N_A^2\,\mathrm{d}\Omega_e}{\displaystyle\sum_{C=1}^{n}\int_{\Omega_e} N_C^2\,\mathrm{d}\Omega_e}\cdot V_e & \text{if } A = B, \\ 0 & \text{otherwise}, \end{cases} \tag{44}$$

n being the number of nodes in the element Ω_e, and $N_\sqcup$ the shape functions.

The question of the scale partition for the VMS methods has been investigated by Holmen et al. [12] through simulations of channel flows. The minimum error regarding the mean velocity profile and the velocity fluctuations is obtained for $\overline{N}/N'$ partitions in the 0.6–0.7 range, with the authors' notations. The fraction of modes in the large-scale space is then given by: $f = \frac{(\overline{N}-1)^2(\overline{N}-2)}{(N'-1)^2(N'-2)}$ (see [11] for details). Henceforth, the range of the k_c/k_c' ratio corresponding to Holmen's studies is approximately 0.2–0.3. This is coherent with Sagaut and Levasseur [13] findings about the spurious pile-up of the resolved kinetic energy which tends to decrease as k_c decreases for a given k_c' since more distant triadic interactions are then accounted for. Furthermore, thanks to the non-orthogonal operator used to separate scales, which enables

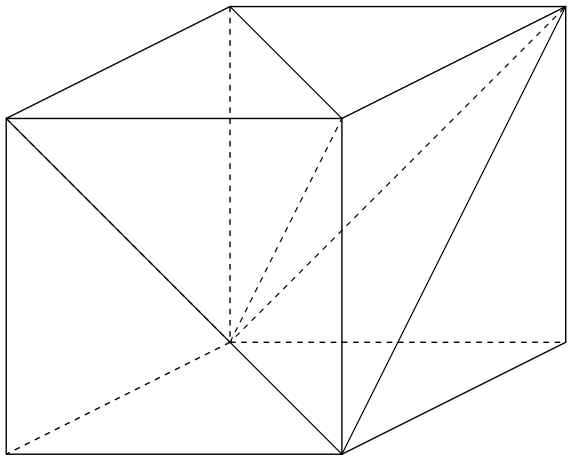

Fig. 2. Schematic of the unstructured mesh used for the computations of isotropic turbulence: from 1 cube, 6 tetrahedra are obtained.

a frequency overlap between the two parts of the resolved flowfield, it could be expected that more modes could be incorporated into the large-scale space, or equivalently a larger k_c/k'_c ratio could be kept.

We choose herein to take for Δ'' the characteristic length of the macro-element obtained by assembling all the elements that share a given node. In practice $\Delta'' = \Delta''_A$ is defined as the cube root of the macro-element volume associated with the A node. The grid used for the study of a decaying isotropic turbulence is based on a structured mesh split into tetrahedra (see Fig. 2). Since the computation is periodic in the three space directions, it can be estimated that every node is shared between 24 different elements. This leads approximatively to the ratio $k_c/k'_c = 0.35$. By analogy with Lilly's approach for the Smagorinsky constant (see [29]), the constants C_1 and C_2, which appear in the Small–Small and Large–Small closures can be evaluated for a given k_c/k'_c ratio. In our case we obtain: $C_1 = 0.22$ and $C_2 = 0.29$ for a 0.18 value of the Smagorinsky constant. These are the values used in the present study.

4. Results on decaying isotropic turbulence

In this section we present calculations of freely evolving isotropic turbulence carried out on 21^3, 51^3 and 81^3 meshes for infinite Reynolds number. The choice of an extremely coarse grid is justified by the fact that our formulation aims at being applied to industrial computations and therefore needs to prove its robustness. The simulations are initialized according to the procedure described by Erlebacher et al. [30]. We compare the results obtained with both Small–Small and Large–Small closures with those deriving from the Smagorinsky model, with a constant set equal to 0.18, and the dynamic Smagorinsky. The choice of this value of the constant will be discussed in Section 4.2. The turbulent Prandtl number is set constant, equal to 0.9. A set of calculations without any subgrid model but with the numerical stabilization has first been computed in order to assess the ability of the Galerkin/least-squares formulation to perform implicit large-eddy simulation (ILES).

4.1. ILES computations

Analytical and numerical studies show that, in the limit of vanishing viscosity, enstrophy can blow up at finite time under particular circumstances detailed in [31], and the kinetic energy spectrum follows a k^2 rule. The stabilization technique implemented in the code prevents enstrophy from blowing up, nevertheless a few other interesting features can be recovered in this case in order to assess our numerical formulation.

Instead of blowing up, the time evolution of enstrophy, $D = \frac{1}{2}\langle \boldsymbol{w}^2 \rangle$, exhibits a peak such that $\frac{D_{\max}}{D(t=0)} = 16.23$ at $t = 33.93$, in the simulations on the 21^3 mesh. This value is quite close to the critical time when enstrophy blows up in the inviscid case: $t_c = 5.9D(t=0)^{-1/2} \approx 31.01$ for a constant skewness factor equal to 0.4.

Figs. 3 and 4 show the kinetic energy spectra at different times in the computations respectively on 21^3 and 51^3 grids. The k^2 law is quite well recovered by the 21^3 calculation, but numerics seems to be much more dissipative when computing on the finest grid. Indeed, the characteristic time-scale matrix $\boldsymbol{\tau}$ tends to 0 as the characteristic length scale of the grid Δ, and the time step Δt, but the fine grid enables to account for smaller scales. Consequently, the computed gradients have higher values, and the global term representing the stabilization, namely $\widehat{\boldsymbol{A}}_i \boldsymbol{W}_{,i} \boldsymbol{\tau} \widehat{\boldsymbol{A}}_j \widehat{\boldsymbol{V}}_{,j}$, is higher as well.

Nevertheless, whatever the grid, the Kolmogorov $k^{-5/3}$ law for the energy spectrum is not recovered by these calculations, so that the least-squares stabilization cannot be considered as a proper subgrid model. Therefore, it is unable to perform ILES or what has been called *implicit modeling* in the introduction section. In the following, the least-squares dissipation will only be considered as a part of the numerical method and not of the subgrid model.

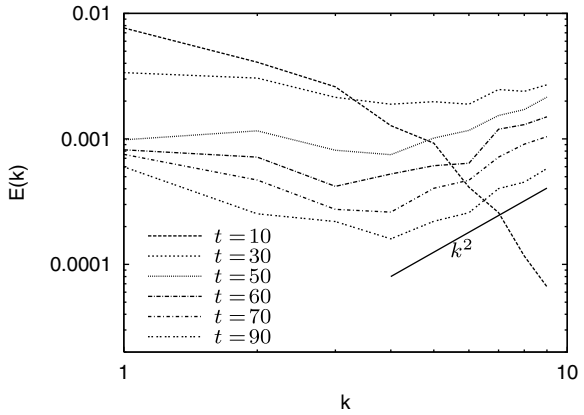

Fig. 3. Resolved kinetic energy spectra at different time of computation on a 21^3 grid with no subgrid model. Straight line indicates a 2 slope.

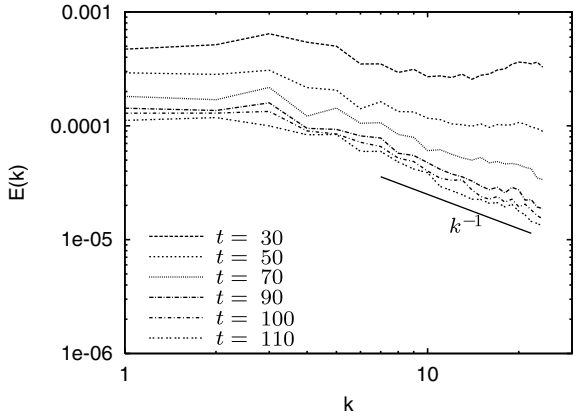

Fig. 4. Resolved kinetic energy spectra at different time of computation on a 51^3 grid with no subgrid model. Straight line indicates a -1 slope.

4.2. Analysis of the VMS closures

The Galerkin/least-squares formulation being not dissipative enough to behave as a subgrid model, the effect of the variational multiscale closures is now investigated. The comparison is done against the Smagorinsky and the dynamic models. Figs. 5 and 6 present the kinetic energy spectra obtained for the different closures at the last step in the simulations. For both grids, the Smagorinsky model reveals an overdissipative behavior for large wavenumbers, i.e., the smallest structures. On the contrary, the dynamic procedure, applied to the same model, correctly accounts for the energy transfers in the whole inertial range. It takes into account the numerical dissipation and computes the right turbulent viscosity. The Kolmogorov law in the inertial range, $E(k) = C_K \varepsilon^{2/3} k^{-5/3}$ is then well reproduced. This is coherent with the time history of the pseudo constant C_d computed by the dynamic procedure, as shown in Fig. 7. The constant stabilizes around 0.1, compared with the 0.18 theoretical value of the Smagorinsky constant. The difference represents the ability of the dynamic procedure to substract from the subgrid model part of the numerical dissipation. Besides, the asymptotic value of the dynamic constant is lower on the fine grid than on the coarse one,

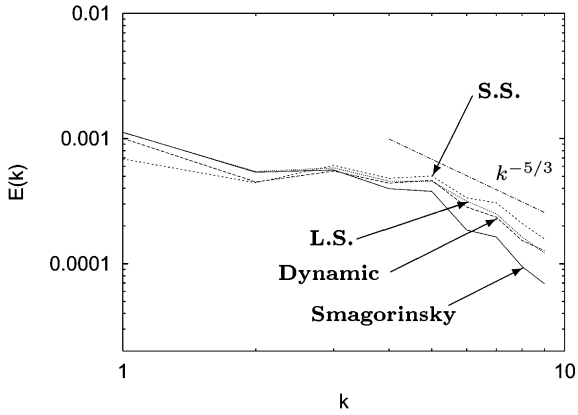

Fig. 5. Turbulent kinetic energy spectra on a 21^3 grid. The subgrid models are Smagorinsky, dynamic, Small–Small and Large–Small. Straight line indicates a $-5/3$ slope.

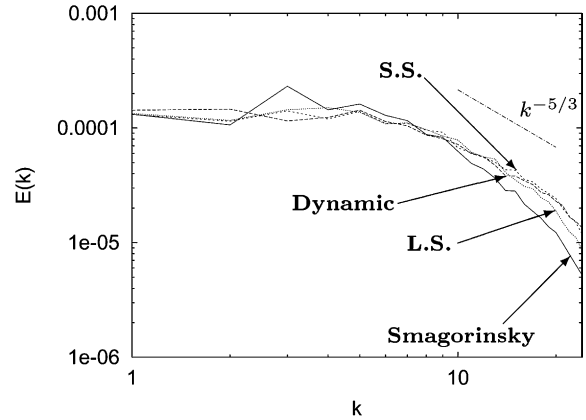

Fig. 6. Turbulent kinetic energy spectra on a 51^3 grid. The subgrid models are Smagorinsky, dynamic, Small–Small and Large–Small. Straight line indicates a $-5/3$ slope.

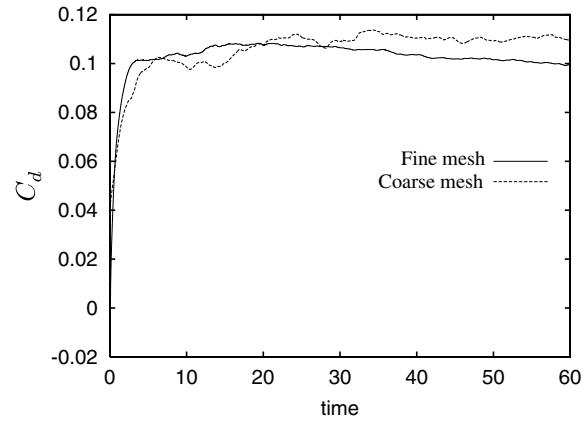

Fig. 7. Time history of the dynamic constant C_d—Fine mesh: 51^3; Coarse mesh: 21^3.

confirming the results of the ILES computations and the fact that the stabilization induces a higher dissipation rate on the finest grid. With this result, we could assume that a Smagorinsky closure with a constant set equal to 0.1 would recover a $k^{-5/3}$ energy spectrum shape. Nonetheless, the value of the constant C_S would greatly depend on the numerical scheme, viz. the finite element formulation as well as the discrete time integration. Moreover, the 0.18 value is known to provide appealing results in the case of isotropic turbulence computed with accurate numerical methods, such as spectral codes, but turns out to be inaccurate when applied to different flows. Therefore, we chose to keep this 0.18 value, corresponding to Lilly's derivation [29], as a reference for the Smagorinsky and VMS closures, rather trying to tune the constant for the particular case of isotropic turbulence, computed in a given numerical framework. Note that previous works on the VMS closures [10,11], used, on the contrary, a Smagorinsky constant set equal to 0.1, as a basis to estimate the VMS constants. Finally, the behavior of the dynamic procedure, and its ability to adapt to a given numerical framework, is highlighted by Fig. 8, which displays the time evolution of the dynamically determined constant computed within different formulations. Additional numerical dissipation has been introduced by adding a discontinuity capturing operator (see [20] for details). On the other hand, the effect of the least-squares stabilization has been lowered by dividing the characteristic time-scale matrix by 2, and 4. The model reacts as expected by lowering the constant when the numerical viscosity increases, namely when the discontinuity capturing operator is plugged in, whereas it tends to increase it when the stabilizing effect diminishes. Nonetheless, this conclusion must be tempered considering the works of Tejada-Martinez et al. [32,33], indicating an inability of the dynamic procedure to adapt to a streamline upwind/Petrov–Galerkin stabilization in an incompressible flow.

Both VMS closures, because they reduce the support of the subgrid viscosity by modifying the dependency of the closure on the largest scales, also provide satisfactory results, very close to the dynamic model. A close look at Fig. 6 still underlines a slight damping of the highest resolved frequencies, namely the last 4 modes, even for the dynamic and VMS models.

At last, the kinetic-energy spectra, computed on a 81^3 grid with the Smagorinsky and VMS Small–Small closures are drawn on Fig. 9 in order to assess the sensitivity of a grid refinement. The multiscale closure improves greatly the result with respect to the Smagorinsky model, even if a slight damping of the highest frequencies is still observed. This confirms the good results obtained on coarse grids, and allows us to think that the statistics and spectra computed with the VMS/GLS formulation may not be affected by a grid refinement.

Fig. 10 represents the time evolution of enstrophy, confirming the presence of more energetic small structures for the dynamic and VMS models. The dynamic model exhibits a peak of enstrophy of amplitude:

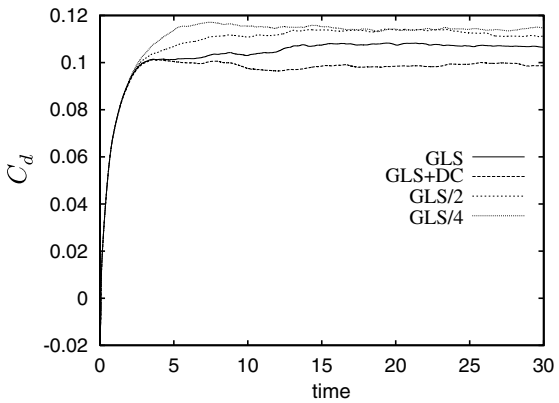

Fig. 8. Time history of the dynamic constant C_d computed through different dissipative formulations.

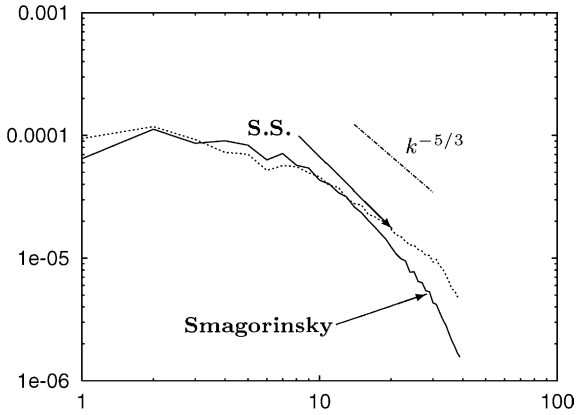

Fig. 9. Turbulent kinetic energy spectra with Smagorinsky and VMS Small–Small closures on a 81^3 grid. Straight line indicates a $-5/3$ slope.

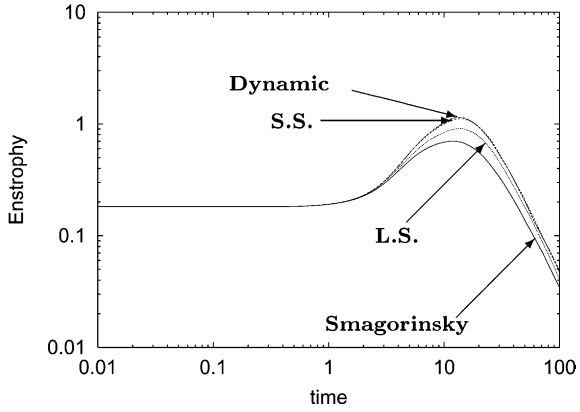

Fig. 10. Time history of resolved enstrophy, 51^3.

$\frac{D_{\max}}{D(t=0)} = 6.3$. The maximum of enstrophy is obtained at $t_c = 13.56$ whereas, in the inviscid case, the critical time when enstrophy blows up is equal to $5.9D(t=0)^{-1/2} \approx 13.83$, for the 51^3 mesh.

4.3. Sensitivity of the scale partition

The kinetic energy spectra obtained with the Small–Small closure for different scale partitioning is presented on Fig. 11. When the k_c/k_c' ratio decreases, the model tends to be overdissipative. In the limit $k_c/k_c' \simeq 0$ it is nothing but the usual Smagorinsky model. On the contrary, for $k_c/k_c' \geqslant 0.5$, despite the Gaussian filter that spreads dissipation over the whole resolved modes, the energy cascade is underpredicted, and the flow hardly sees the subgrid model.

4.4. Comparison between numerical and subgrid dissipation

It has already been underlined that a key point in developing an effective subgrid model is its ability to adapt to a given numerical framework. In an industrial context, constraints are strong to have a robust

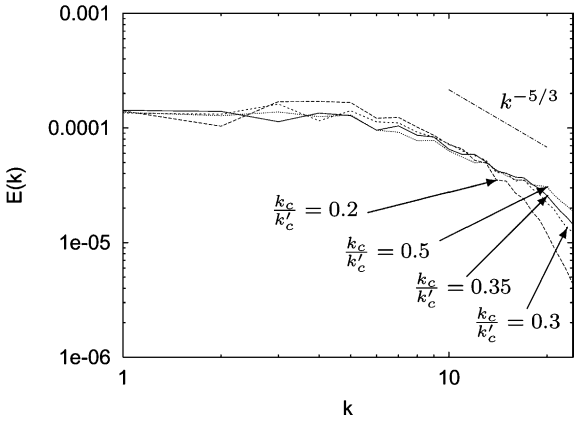

Fig. 11. Sensitivity of the scale partition for the VMS Small–Small closure, 51^3.

code and imply the use of sophisticated stabilization techniques. Effects of the different sources of dissipation are now investigated. Figs. 12–14 represent the spectral density of probability of both the subgrid dissipation and the dissipation due to the least-squares stabilization, respectively on the 21^3, 51^3 and 81^3 grids. The subgrid energy dissipation rate is calculated as: $\varepsilon_{\text{sgs}} = \rho u_i \nabla \cdot \tau_{s_{ij}}$. It is worth noting that the least-squares stabilization acts on the momentum equations as well as the continuity and energy equations. Nevertheless, only the contribution on the momentum equations is taken into account here to make a relevant comparison with the subgrid dissipation. Thus, the least-squares dissipation is assessed as

$$\varepsilon_{\text{gls}} = \sum_{k=2}^{4} \left[\boldsymbol{U}^n \rfloor_k \cdot \int_{\Omega(n)} \left(\widehat{\boldsymbol{A}}_{,i} N_{,i} \boldsymbol{\tau} (\widehat{\boldsymbol{A}}_0 \widehat{\boldsymbol{V}}_{,t} + \widehat{\boldsymbol{A}}_j \widehat{\boldsymbol{V}}_{,j}) \right) \Big|_k \mathrm{d}\Omega(n) \right] \tag{45}$$

where $\rfloor_k$ denotes the kth component of the considered vector, $\boldsymbol{U}^n$ is the $\boldsymbol{U}$-vector at node n, N is the shape function associated with the node n, and $\Omega(n)$ is the set of all the elements that contain node n.

The dissipation spectra in Figs. 12–14 are normalized by the mean of the root mean square of total dissipation obtained by each simulation. It enables to compare not only the shapes of the spectra but also the relative levels of dissipation for each grid.

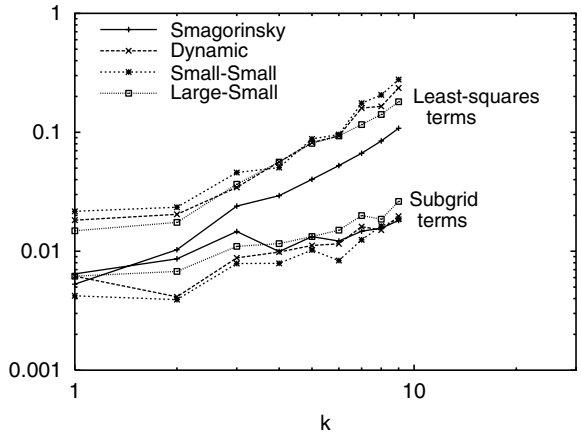

Fig. 12. Comparison of least-squares and subgrid dissipation spectra for the different models, 21^3.

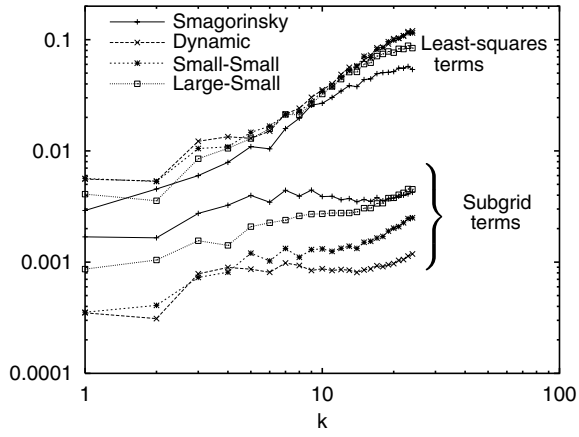

Fig. 13. Comparison of least-squares and subgrid dissipation spectra for the different models, 51^3.

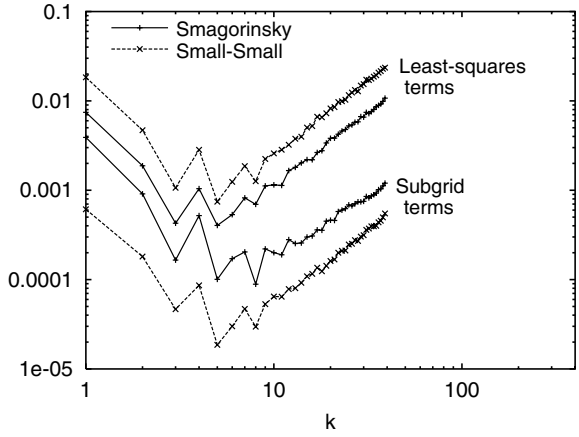

Fig. 14. Comparison of least-squares and subgrid dissipation spectra for the Smagorinsky and VMS Small–Small closures, 81^3.

It appears clear that for all simulations, the dissipation due to the numerical formulation dominates the subgrid effects! Garnier et al. [34] already underlined this fact with the generalized Smagorinsky constant concept. Despite the relatively weak importance of the subgrid dissipation in front of the numerical dissipation, a variation on the subgrid model has been seen to yield different results: the effect of subgrid modelization is obviously not negligible. This is also coherent with ILES computations, which were not dissipative enough, with a resolved kinetic energy decay rate higher than $-5/3$.

The shape of least-squares and subgrid-dissipation spectra are also rather different from each other. The subgrid models give raise to a dissipation spectrum of the form $k^2E(k) \propto k^{1/3}$ while the least-squares dissipation spectrum is rather of the form $k^{4/3}$. The numerical formulation used here tends to over-dissipate the small scales, confirming that it cannot perform ILES. Besides, as already mentioned, the computations show that the least-squares dissipation is much more sensitive to the mesh than a subgrid closure.

A very interesting point for the variational multiscale approach is that it automatically incorporates some information on the numerical dissipation, since the closures depend on the high frequency part of the resolved field. Thus, in presence of another source of small-scale damping, the computed turbulent

viscosity will diminish and provide the right correction. This is typically the behavior expected from the Germano and Lilly's dynamic procedure. Comparison of Figs. 12 and 13 shows the translation of the subgrid dissipation spectra of dynamic and VMS models on the 51^3 grid, namely when the numerical dissipation is higher with respect to the calculation on the 21^3 grid.

At last, it is worth noting that the least-squares dissipation is lower with the Smagorinsky model than with the other closures, since this model induces too high a damping of the smallest scales. Therefore, the computed gradients in the expression of the least-squares stabilization term are weaker.

Figs. 15–17 represent the equivalent effective viscosity of both dissipation, respectively: $v_{e_{\text{sgs}}} = \varepsilon_{\text{sgs}}/2k^2 E(k)$ and $v_{e_{\text{gls}}} = \varepsilon_{\text{gls}}/2k^2 E(k)$. This can be compared with the work of Domaradzki et al. [35] who proposed a method for computing effective numerical eddy viscosity, evaluated on the non-oscillatory finite volume scheme MPDATA.

Eventually, the coherence between GLS and subgrid dissipation is drawn in Figs. 18 and 19 for both mesh sizes.

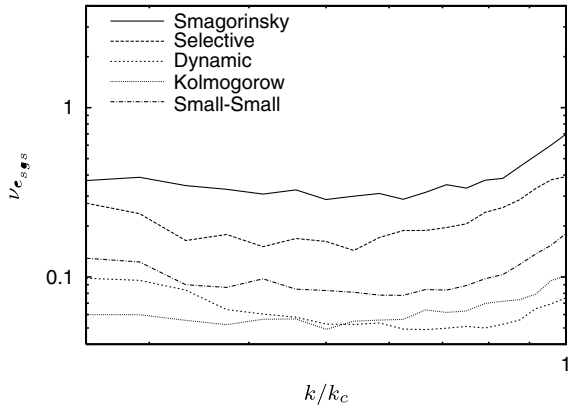

Fig. 15. Effective viscosity corresponding to the subgrid kinetic energy dissipation rate, 51^3.

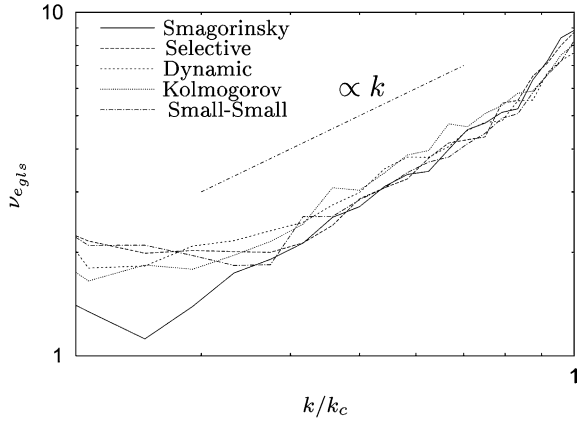

Fig. 16. Effective viscosity corresponding to the least-squares stabilization, 51^3.

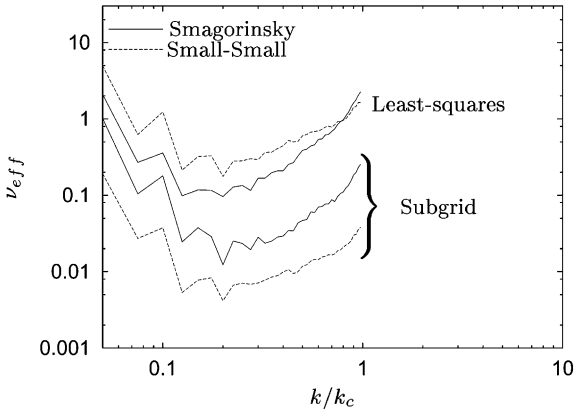

Fig. 17. Effective viscosity, 81^3.

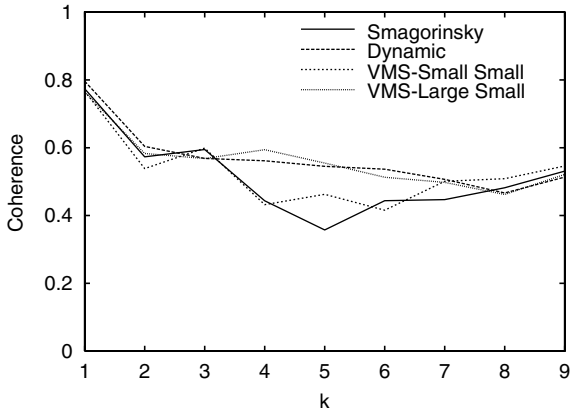

Fig. 18. Coherence of least-squares and subgrid dissipation, 21^3.

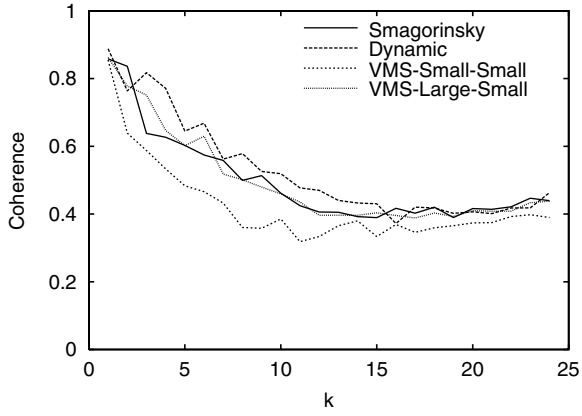

Fig. 19. Coherence of least-squares and subgrid dissipation, 51^3.

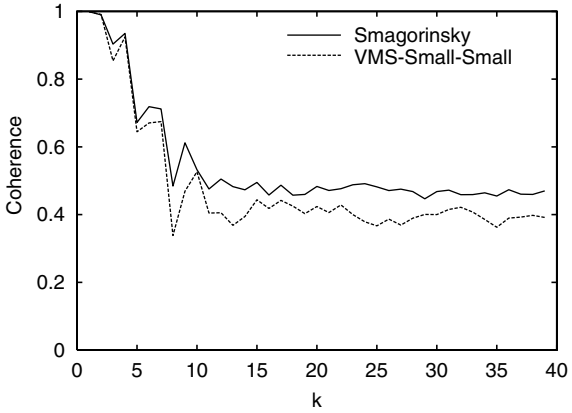

Fig. 20. Coherence of least-squares and subgrid dissipation, 81^3.

It is defined as

$$C(\varepsilon_{\mathrm{gls}}, \varepsilon_{\mathrm{sgs}}) = \frac{\displaystyle\int_{\|\boldsymbol{k}\|} \varepsilon_{\mathrm{gls}} \varepsilon^*_{\mathrm{sgs}} \, \mathrm{d}\boldsymbol{k}}{\displaystyle\sqrt{\int_{\|\boldsymbol{k}\|} \varepsilon_{\mathrm{gls}} \varepsilon^*_{\mathrm{gls}} \, \mathrm{d}\boldsymbol{k} \int_{\|\boldsymbol{k}\|} \varepsilon_{\mathrm{sgs}} \varepsilon^*_{\mathrm{sgs}} \, \mathrm{d}\boldsymbol{k}}}, \tag{46}$$

where $\varepsilon_{\mathrm{gls}}$ and $\varepsilon_{\mathrm{sgs}}$ are respectively the GLS and subgrid dissipation in the Fourier space, and $C(\varepsilon_{\mathrm{gls}}, \varepsilon_{\mathrm{sgs}})$ is the coherence coefficient (Fig. 20).

Beside the different levels of dissipation brought by each model, the spectral behavior turns out to be also very important, and consequently the energy-transfer mechanisms are not described in the same manner.

5. Conclusions

The variational multiscale approach has been investigated in physical space based on simulations of freely evolving isotropic turbulence. The hyperviscosity formulation of the VMS on unstructured meshes is detailed and yields good results. It correctly balances the kinetic energy transfers taking into account the dissipation coming from the GLS stabilization technique. Furthermore, this approach can easily be implemented and proves efficient. It represents an increase of the CPU time of only 20% with respect to the Smagorinsky model, while the dynamic procedure involves an increase of almost 35%. Eventually, the VMS approach, as implemented, can be extended to complex flows without restrictions on homogeneity directions, unlike the dynamic model because of its instability problem.

Acknowledgment

This work was supported by the French Ministry of Defense through a D.G.A. fellowship (Délégation Générale pour l'Armement).

Appendix A. Filtered equations of a turbulent compressible flow

The compressible Navier–Stokes equations for a perfect gas are

$$\begin{aligned}
&\frac{\partial \rho}{\partial t}+\frac{\partial \rho u_j}{\partial x_j}=0,\\
&\frac{\partial \rho u_i}{\partial t}+\frac{\partial \rho u_i u_j}{\partial x_j}+\frac{\partial p}{\partial x_i}=\frac{\partial \sigma_{ij}}{\partial x_j},\\
&\frac{\partial \rho E}{\partial t}+\frac{\partial \rho E u_j}{\partial x_j}+\frac{\partial p u_j}{\partial x_j}=\frac{\partial \sigma_{ij}u_i}{\partial x_j}-\frac{\partial q_j}{\partial x_j}.
\end{aligned} \tag{47}$$

The filtered counterpart of Eq. (47) is obtained using the mass-weighted change of variables defined on a variable ϕ as $\tilde{\phi}=\overline{\rho\phi}/\bar{\rho}$. In order to keep time-dependent integration quantities, Lee [36] substitutes the filtered total energy equation $\overline{\rho E}=\bar{\rho}\widetilde{E}=\bar{p}/(\gamma-1)+\frac{1}{2}\bar{\rho}\widetilde{u_i u_i}$ by the transport equation of the computable energy:

$$\bar{\rho}\check{E}=\frac{\bar{p}}{\gamma-1}+\frac{1}{2}\bar{\rho}\tilde{u}_i\tilde{u}_i=\bar{\rho}\widetilde{E}-\frac{1}{2}\tau_{ii}, \tag{48}$$

where $\tau_{ij}=\bar{\rho}\widetilde{u_i u_j}-\bar{\rho}\tilde{u}_i\tilde{u}_j$ is the subgrid tensor.

If the filtering of the momentum equations appears quite classic, by the introduction of a subgrid tensor similar as the one introduced for incompressible flows, there remain several approaches for the filtered energy equation. One can cite for instance the works of Vreman [37] or Sreedhar and Raghab [38]. Following the results of Vreman et al. [21] within the context of a priori tests on DNS of a temporal mixing layer, the non-linearity associated with viscous stress and heat flux are assumed negligible. Yoshizawa [39], as well as Moin et al. [40] proposed a modelization for the trace of the subgrid tensor. Ducros et al. [41] introduce a macro-temperature incorporating the trace of the subgrid tensor, by reference to the macro-pressure of Métais and Lesieur [42]. The approach used in our case consists merely in neglecting the trace of the subgrid tensor, advocating as proposed by Erlebacher et al. [43,44] that $\tau_{kk}=\gamma M_{\mathrm{sgs}}^2\bar{p}$ and M_{sgs} the subgrid Mach number is small when the considered infinite Mach number is not too large. More precisely, the authors highlight that the thermodynamic pressure will be much more important when the subgrid Mach number is lower than 0.4, or equivalently for turbulent Mach numbers up to 0.6. This latter condition incorporates a major part of supersonic flows. This was quite well verified by Ducros et al. [41], but Moin et al. [40] found that the subgrid energy represents 40% of the thermodynamic pressure when considering turbulent Mach numbers around 0.35. This enables, however, to keep in the equations a non-modified pressure, and it also leads to: $\bar{\rho}\widetilde{E}\simeq\bar{\rho}\check{E}$. Besides, in order to take into account the subgrid stress appearing in the momentum equations, the associated work is explicitely introduced in the total energy equation.

Therefore, the filtered equations resolved herein are

$$\frac{\partial \bar{\rho}}{\partial t}+\frac{\partial \bar{\rho}\tilde{u}_j}{\partial x_j}=0, \tag{49}$$

$$\frac{\partial \bar{\rho}\tilde{u}_i}{\partial t}+\frac{\partial \bar{\rho}\tilde{u}_i\tilde{u}_j}{\partial x_j}+\frac{\partial \bar{p}}{\partial x_i}=\frac{\partial}{\partial x_j}[2\tilde{\mu}\widetilde{S}_{ij}]-\frac{\partial \tau_{ij}^d}{\partial x_j}, \tag{50}$$

$$\frac{\partial \bar{\rho}\check{E}}{\partial t}+\frac{\partial \bar{\rho}\check{E}\tilde{u}_j}{\partial x_j}+\frac{\partial \bar{p}\tilde{u}_j}{\partial x_j}=\frac{\partial}{\partial x_j}\left[2\tilde{\mu}\widetilde{S}_{ij}\tilde{u}_i\right]+\frac{\partial}{\partial x_j}\left[\tilde{\kappa}\frac{\partial \widetilde{T}}{\partial x_j}\right]-\frac{\partial Q_j}{\partial x_j}-\frac{\partial \tau_{ij}^d u_i}{\partial x_j}, \tag{51}$$

with $Q_j=(\overline{\rho E u_j}-\bar{\rho}\widetilde{E}\tilde{u}_j)+(\overline{p u_j}-\bar{p}\tilde{u}_j)-\tau_{ij}^d\tilde{u}_i$ and $\tau_{ij}^d=\tau_{ij}-\frac{1}{3}\tau_{kk}\delta_{ij}$, the deviatoric part of the subgrid tensor, that both need to be modeled.

For non-VMS models, the subgrid stress is modeled within a turbulent viscosity hypothesis:

$$\tau_{ij}^d=-2\mu_t\widetilde{S}_{ij}, \tag{52}$$

and the vector Q_j is modeled with reference to the heat flux:

$$Q_j = -\kappa_t \frac{\partial \widetilde{T}}{\partial x_j}, \qquad \kappa_t = \frac{\gamma c_v \tilde{\mu}_t}{Pr_t}, \tag{53}$$

where μ_t is the eddy-viscosity, κ_t the turbulent heat conductivity and Pr_t the turbulent Prandtl number, set constant and equal to 0.9 for the study.

The filtered perfect gas relation is

$$\bar{p} = \bar{\rho} r \widetilde{T}. \tag{54}$$

Appendix B. Entropy coefficient matrices

The compressible Navier–Stokes equation in conservation variables is

$$\boldsymbol{U}_{,t} + \boldsymbol{A}_i \boldsymbol{U}_{,i} = \left(\boldsymbol{K}_{ij} \boldsymbol{U}_{,j}\right)_{,i}. \tag{55}$$

Let us recall the definition of the change of variables,

$$\boldsymbol{V} = \frac{1}{\rho T} \begin{Bmatrix} -U_5 + \rho c_v T \left(\gamma + 1 - \dfrac{(\gamma-1)s}{r}\right) \\ U_2 \\ U_3 \\ U_4 \\ -U_1 \end{Bmatrix} = \frac{1}{T} \begin{Bmatrix} h - Ts - \dfrac{\|\boldsymbol{u}\|^2}{2} \\ u_1 \\ u_2 \\ u_3 \\ -1 \end{Bmatrix}. \tag{56}$$

In entropy variables, Eq. (55) rewrites

$$\boldsymbol{A}_0 \boldsymbol{V}_{,t} + \widetilde{\boldsymbol{A}}_i \boldsymbol{V}_{,i} = (\widetilde{\boldsymbol{K}}_{ij} \boldsymbol{V}_{,j})_{,i}, \tag{57}$$

with

$$\boldsymbol{V}^{\mathrm{T}} = \frac{\partial \mathscr{H}(\boldsymbol{U})}{\partial \boldsymbol{U}}, \tag{58}$$

$$\widetilde{\boldsymbol{A}}_0 = \boldsymbol{U}_{,V}, \tag{59}$$

$$\widetilde{\boldsymbol{A}}_i = \boldsymbol{A}_i \widetilde{\boldsymbol{A}}_0, \tag{60}$$

$$\widetilde{\boldsymbol{K}}_{ij} = \boldsymbol{K}_{ij} \widetilde{\boldsymbol{A}}_0. \tag{61}$$

Let us denote $k = \frac{1}{2}\|\boldsymbol{u}^2\|$ the specific kinetic energy, $e = c_v T$ the specific internal energy, $\bar{\gamma} = \gamma - 1$, and

$$\begin{aligned} &c_1 = \bar{\gamma} e + u_1^2, \qquad c_2 = \bar{\gamma} e + u_2^2, \qquad c_3 = \bar{\gamma} e + u_3^2, \\ &k_1 = k + \gamma e, \qquad k_2 = k + e, \qquad k_3 = k + (\bar{\gamma} + \gamma) e, \\ &k_4 = k^2 + 2\gamma e k + \gamma e^2, \qquad k_5 = k_4^2 + 2\bar{\gamma} e (k + \gamma e). \end{aligned} \tag{62}$$

The Riemannian metric tensor $\widetilde{\boldsymbol{A}}_0$ is, in term of primitive variables,

$$\widetilde{\boldsymbol{A}}_0 = \frac{\rho}{c_v(\gamma - 1)} \begin{bmatrix} 1 & u_1 & u_2 & u_3 & k_2 \\ & e\bar{\gamma} + u_1^2 & u_1 u_2 & u_1 u_3 & k_1 u_1 \\ & & e\bar{\gamma} + u_2^2 & u_2 u_3 & k_1 u_2 \\ & \text{Symm.} & & e\bar{\gamma} + u_3^2 & k_1 u_3 \\ & & & & k_4 \end{bmatrix}. \tag{63}$$

The advective Jacobians $\widetilde{\boldsymbol{A}}_i$ read:

$$\widetilde{\boldsymbol{A}}_1 = \frac{\rho}{c_v(\gamma-1)}\begin{bmatrix} u_1 & c_1 & u_1u_2 & u_1u_3 & k_1u_1 \\ & (2\bar{\gamma}e+c_1)u_1 & c_1u_2 & c_1u_3 & c_1k_1+\bar{\gamma}eu_1^2 \\ & & c_2u_1 & u_1u_2u_3 & k_3u_1u_2 \\ & \text{Symm.} & & c_3u_1 & k_3u_1u_3 \\ & & & & k_5u_1 \end{bmatrix}, \tag{64}$$

$$\widetilde{\boldsymbol{A}}_2 = \frac{\rho}{c_v(\gamma-1)}\begin{bmatrix} u_2 & u_1u_2 & c_2 & u_2u_3 & k_1u_2 \\ & c_1u_2 & c_2u_1 & u_1u_2u_3 & k_3u_1u_2 \\ & & (2\bar{\gamma}e+c_2)u_2 & c_2u_3 & c_2k_1+\bar{\gamma}eu_2^2 \\ & \text{Symm.} & & c_3u_2 & k_3u_2u_3 \\ & & & & k_5u_2 \end{bmatrix}, \tag{65}$$

$$\widetilde{\boldsymbol{A}}_3 = \frac{\rho}{c_v(\gamma-1)}\begin{bmatrix} u_3 & u_1u_3 & u_2u_3 & c_3 & k_1u_3 \\ & c_1u_3 & u_1u_2u_3 & c_3u_1 & k_3u_1u_3 \\ & & c_2u_3 & c_3u_2 & k_3u_2u_3 \\ & \text{Symm.} & & (2\bar{\gamma}e+c_3)u_3 & c_3k_1+\bar{\gamma}eu_3^2 \\ & & & & k_5u_3 \end{bmatrix}. \tag{66}$$

The diffusive fluxes are given as

$$\boldsymbol{F}_i^{\text{diff}} = \begin{Bmatrix} 0 \\ \sigma_{1i} \\ \sigma_{2i} \\ \sigma_{3i} \\ \sigma_{ij}u_j - q_i \end{Bmatrix}, \tag{67}$$

where $\sigma_{ij} = \mu(u_{i,j} + u_{j,i}) + \lambda u_{k,k}\delta_{ij}$ and $q_i = -\kappa T_{,i}$.

The velocity components and temperature are written as

$$\tilde{u}_i = -\frac{\widehat{\boldsymbol{V}}_{i+1}}{\widehat{\boldsymbol{V}}_5}, \tag{68}$$

$$\widetilde{T} = -\frac{1}{\widehat{\boldsymbol{V}}_5}. \tag{69}$$

Let us denote $\chi = \lambda + 2\mu$, the diffusivity matrices defined as $\widetilde{\boldsymbol{K}}_{ij}\boldsymbol{V}_{,j} = \boldsymbol{F}_i^{\text{diff}}$ are then written, in term of primitive variables as

$$\widetilde{\boldsymbol{K}}_{11}(\mu,\lambda,\kappa,\boldsymbol{U}) = T\begin{bmatrix} 0 & 0 & 0 & 0 & 0 \\ 0 & \chi & 0 & 0 & \chi u_1 \\ 0 & 0 & \mu & 0 & \mu u_2 \\ 0 & 0 & 0 & \mu & \mu u_3 \\ 0 & \chi u_1 & \mu u_2 & \mu u_3 & \chi u_1^2 + \mu\left(u_2^2+u_3^2\right) + \dfrac{\mu c_p}{Pr}T \end{bmatrix}, \tag{70}$$

$$\widetilde{\boldsymbol{K}}_{22}(\mu,\lambda,\kappa,\boldsymbol{U}) = T\begin{bmatrix} 0 & 0 & 0 & 0 & 0 \\ 0 & \mu & 0 & 0 & \mu u_1 \\ 0 & 0 & \chi & 0 & \chi u_2 \\ 0 & 0 & 0 & \mu & \mu u_3 \\ 0 & \mu u_1 & \chi u_2 & \mu u_3 & \chi u_2^2 + \mu\left(u_1^2+u_3^2\right) + \dfrac{\mu c_p}{Pr}T \end{bmatrix}, \tag{71}$$

$$\widetilde{\boldsymbol{K}}_{33}(\mu,\lambda,\kappa,\boldsymbol{U}) = T\begin{bmatrix} 0 & 0 & 0 & 0 & 0 \\ 0 & \mu & 0 & 0 & \mu u_1 \\ 0 & 0 & \mu & 0 & \mu u_2 \\ 0 & 0 & 0 & \chi & \chi u_3 \\ 0 & \mu u_1 & \mu u_2 & \chi u_3 & \chi u_3^2 + \mu\left(u_1^2+u_2^2\right) + \dfrac{\mu c_p}{Pr}T \end{bmatrix}, \tag{72}$$

$$\widetilde{\boldsymbol{K}}_{12}(\mu,\lambda,\kappa,\boldsymbol{U}) = \widetilde{\boldsymbol{K}}_{21}^{\mathrm{T}} = T\begin{bmatrix} 0 & 0 & 0 & 0 & 0 \\ 0 & 0 & \lambda & 0 & \lambda u_2 \\ 0 & \mu & 0 & 0 & \mu u_1 \\ 0 & 0 & 0 & 0 & 0 \\ 0 & \mu u_2 & \lambda u_1 & 0 & (\lambda+\mu)u_1u_2 \end{bmatrix}, \tag{73}$$

$$\widetilde{\boldsymbol{K}}_{13}(\mu,\lambda,\kappa,\boldsymbol{U}) = \widetilde{\boldsymbol{K}}_{31}^{\mathrm{T}} = T\begin{bmatrix} 0 & 0 & 0 & 0 & 0 \\ 0 & 0 & 0 & \lambda & \lambda u_3 \\ 0 & 0 & 0 & 0 & 0 \\ 0 & \mu & 0 & 0 & \mu u_1 \\ 0 & \mu u_3 & 0 & \lambda u_1 & (\lambda+\mu)u_1u_3 \end{bmatrix}, \tag{74}$$

$$\widetilde{\boldsymbol{K}}_{23}(\mu,\lambda,\kappa,\boldsymbol{U}) = \widetilde{\boldsymbol{K}}_{32}^{\mathrm{T}} = T\begin{bmatrix} 0 & 0 & 0 & 0 & 0 \\ 0 & 0 & 0 & 0 & 0 \\ 0 & 0 & 0 & \lambda & \lambda u_3 \\ 0 & 0 & \mu & 0 & \mu u_2 \\ 0 & 0 & \mu u_3 & \lambda u_2 & (\lambda+\mu)u_2u_3 \end{bmatrix}. \tag{75}$$

In practice, Stokes' hypothesis is assumed, i.e., $\lambda + 2/3\mu = 0$.

The subgrid diffusivity matrices for LES and variational multiscale LES are easily derived from these expressions: $\widehat{\boldsymbol{K}}_{ij}^{\mathrm{SGS}}$ (see Eq. (21)) is obtained by replacing μ and Pr respectively by μ_t and Pr_t and $\boldsymbol{K}_{ij}^{VMS}$ (see Eq. (39)) is obtained by replacing μ, Pr and u_i respectively by μ_t, Pr_t and $u_i'' = -\frac{\Delta''}{24}u_{i,kk}$.

References

[1] K. Jansen, Preliminary large-eddy simulations of flow over a NACA 4412 airfoil using unstructured grids, Annual Research Briefs, Center for Turbulence Research, NASA Ames/Stanford University, 1995, p. 61.

[2] F. Chalot, B. Marquez, M. Ravachol, F. Ducros, F. Nicoud, Th. Poinsot, A consistent finite element approach to large eddy simulation, AIAA Paper 98-2652, 1998.

[3] D. Knight, G. Zhou, N. Okong'o, V. Shukla, Compressible large eddy simulation using unstructured grids, AIAA Paper 98-0535, 1998.

[4] N. Okong'o, D. Knight, Compressible large eddy simulation using unstructured grids: channel and boundary layer flows, AIAA Paper 98-3315, 1998.

[5] G. Urbin, D. Knight, A.A. Zheltovodov, Compressible large eddy simulation using unstructured grids: supersonic turbulent boundary layer and compression corner, AIAA Paper 99-0427, 1999.

[6] G. Urbin, D. Knight, A.A. Zheltovodov, Large eddy simulation of a supersonic compression corner part I, AIAA Paper 2000-0398, 2000.
[7] T.A. Simons, R.H. Pletcher, Large eddy simulation of turbulent flows using unstructured grids, AIAA Paper 98-3314, 1998.
[8] T.J.R. Hughes, J.R. Stewart, A space-time formulation for multiscale phenomena, J. Comput. Appl. Math. 74 (1996) 217.
[9] T.J.R. Hughes, L. Mazzei, K.E. Jansen, Large eddy simulation and the variational multiscale method, Comput. Visual Sci. 3 (2000) 47.
[10] T.J.R. Hughes, L. Mazzei, A.A. Oberai, The multiscale formulation of large eddy simulation: decay of homogeneous isotropic turbulence, Phys. Fluids 13 (2001) 505.
[11] T.J.R. Hughes, A.A. Oberai, L. Mazzei, Large eddy simulation of turbulent channel flows by the variational multiscale method, Phys. Fluids 13 (2001) 1784.
[12] J. Holmen, T.J.R. Hughes, A.A. Oberai, G.N. Wells, Sensitivity of the scale partition for variational multiscale large-eddy simulation of channel flow, Phys. Fluids 16 (2004) 824.
[13] P. Sagaut, V. Levasseur, Sensitivity of spectral variational multiscale methods for large-eddy simulation of isotropic turbulence, Phys. Fluids, in press.
[14] G. Winckelmans, H. Jeanmart, Assessment of some models for LES without and with explicit filtering, in: B.J. Geurts, R. Friedrich, O. Métais (Eds.), Direct and Large-eddy Simulation IV, ERCOFTAC Series, Kluwer, Dordrecht, 2001, p. 55.
[15] B. Koobus, C. Farhat, A variational multiscale method for the large-eddy simulation of compressible turbulent flows on unstructured meshes–Application to vortex shedding, Comput. Methods Appl. Mech. Engrg. 193 (2004) 1367.
[16] K. E. Jansen, A. E. Tejada-Martinez, An evaluation of the variational multiscale method for large-eddy simulation while using a hierarchical basis, AIAA Paper 2002-3124, 2002.
[17] T.J.R. Hughes, L.P. Franca, M. Mallet, A new finite element formulation for computational fluid dynamics: I. Symmetric forms of the compressible Euler and Navier–Stokes equations and the second law of thermodynamics, Comput. Methods Appl. Mech. Engrg. 54 (1986) 223.
[18] P. Sagaut, Large Eddy Simulation for Incompressible Flow: an Introduction, Springer, Berlin, 2002.
[19] M. Mallet, A finite element method for computational fluid dynamics, Ph.D. Thesis, Stanford College, 1985.
[20] F. Shakib, Finite element analysis of the compressible Euler and Navier–Stokes equations, Ph.D. Thesis, Stanford College, 1989.
[21] B. Vreman, B. Geurts, H. Kuerten, A priori tests of large eddy simulation of the compressible plane mixing layer, J. Engrg. Math. 29 (1995) 299.
[22] K.E. Jansen, C. Whiting, S. Collis, F. Shakib, A better consistency for low-order stabilized finite element methods, Comput. Methods Appl. Mech. Engrg. 174 (1999) 153.
[23] T.J.R. Hughes, M. Mallet, A new finite element formulation for computational fluid dynamics: III. The generalized streamline operator for multidimensional advective–diffusive systems, Comput. Methods Appl. Mech. Engrg. 58 (1986) 305.
[24] S.B. Pope, Turbulent Flows, Cambridge University Press, Cambridge, 2000.
[25] J. Smagorinsky, General circulation experiments with the primitive equations, the basic experiment, Mon. Weather Rev. (1963) 92.
[26] M. Germano, U. Piomelli, P. Moin, W.H. Cabot, A dynamic subgrid-scale eddy viscosity model, Phys. Fluids A 3 (1991) 1760.
[27] A.W. Vreman, The filtering analog of the variational multiscale method in large-eddy simulation, Phys. Fluids A 15 (8) (2003) L61.
[28] T.J.R. Hughes, The Finite Element Method: Linear Static and Dynamic Finite Element Analysis, Prentice-Hall, Englewood Cliffs, NJ, 1987.
[29] D.K. Lilly, On the application of the eddy-viscosity concept in the inertial subrange of turbulence, Manuscript 123, NCAR, Boulder, CO, 1966.
[30] G. Erlebacher, M.Y. Hussaini, H.O. Kreiss, S. Sarkar, The analysis and simulation of compressible turbulence, Theoret. Comput. Fluid Dyn. 2 (1990) 73.
[31] M. Lesieur, Turbulence in Fluids, third ed., Kluwer Academic Publishers, Dordrecht, 1997.
[32] A.E. Tejada-Martinez, Dynamic subgrid-scale modeling for large-eddy simulation of turbulent flows with a stabilized finite element method, Ph.D. Thesis, Scientific Computation Research Center, Rensselaer Polytechnic Institute, 2003.
[33] A.E. Tejada-Martinez, K.E. Jansen, On the interaction between dynamic model dissipation and numerical dissipation due to streamline upwind/Petrov–Galerkin stabilization, Comput. Methods Appl. Mech. Engrg. 194 (9) (2005) 1225.
[34] E. Garnier, M. Mosse, P. Sagaut, M. Deville, P. Comte, On the use of shock-capturing schemes for large-eddy simulation, J. Comput. Phys. 153 (1999) 273.
[35] J.A. Domaradzki, Z. Xiao, P.K. Smolarkiewicz, Effective eddy viscosities in implicit large eddy simulations of turbulent flows, Phys. Fluids 15 (2003) 3890.
[36] S. Lee, Large-eddy simulation of shock turbulence interaction, in: Annual Research Briefs, Center for Turbulence Research, Stanford, CA, 1992, p. 73.
[37] A.W. Vreman, Direct and Large Eddy Simulation of the compressible turbulent mixing layer, Ph.D. Dissertation, University of Twente, Twente, 1995.

[38] M. Sreedhar, S. Raghab, Large eddy simulation of longitudinal stationary vortices, Phys. Fluids 6 (1994) 2501.
[39] Y. Yoshizawa, Statistical theory for compressible turbulent shear flows with the application to subgrid modeling, Phys. Fluids 29 (1986) 2152.
[40] P. Moin, K. Squires, W. Cabot, S. Lee, A dynamic subgrid-scale model for compressible turbulence and scalar transport, Phys. Fluids A 3 (1991) 2746.
[41] F. Ducros, P. Comte, M. Lesieur, Large-eddy simulation of transition to turbulence in a boundary layer developing spatially over a flat plate, J. Fluid. Mech. 326 (1996) 1.
[42] O. Métais, M. Lesieur, Spectral large-eddy simulation of isotropic and stably stratified turbulence, J. Fluid Mech. 239 (1992) 157.
[43] G. Erlebacher, M.Y. Hussaini, C.G. Speziale, T.A. Zang, Toward the large eddy simulation of compressible turbulent flow, ICASE Report No. 87-20, 1987.
[44] G. Erlebacher, M.Y. Hussaini, C.G. Speziale, T.A. Zang, Toward the large eddy simulation of compressible turbulent flow, J. Fluid Mech. 238 (1992) 155.